

# Transverse Single-Spin Asymmetry and Cross Section for $\pi^0$ and $\eta$ Mesons at Large Feynman- $x$ in $\sqrt{s} = 200$ GeV $p^\uparrow + p$ Collisions

(Dated: August 17, 2011)

We present STAR measurements of the differential cross section and transverse single-spin asymmetry ( $A_N$ ) vs. Feynman- $x$  ( $x_F$ ) for  $\pi^0$  and  $\eta$  mesons, for  $0.4 < x_F < 0.75$  at an average pseudorapidity of 3.68. A data sample during  $p + p$  collisions at  $\sqrt{s} = 200$  GeV of approximately  $6.8 \text{ pb}^{-1}$  was recorded with an average beam polarization of about 56 %. The cross section for  $\pi^0$  is consistent with a perturbative QCD prediction, and the  $\eta/\pi^0$  cross-section ratio agrees with previous mid-rapidity measurements.  $A_N$  for  $\eta$  is found to be significantly larger than the already large  $A_N$  for  $\pi^0$ .

PACS numbers:

A well known prediction of collinear perturbative Quantum Chromo Dynamics (pQCD) is that the cross section for forward meson production in proton-proton collisions should have negligible dependence on the transverse polarization of the incident proton [1]. This early prediction was contradicted by measurements [2, 3] of sizable pion transverse single-spin asymmetries ( $A_N$ ), defined for a forward moving polarized beam scattering to the left and with a vertical spin quantization axis,

$$A_N \equiv \frac{\sigma^\uparrow - \sigma^\downarrow}{\sigma^\uparrow + \sigma^\downarrow}. \quad (1)$$

In order to explain the large asymmetries, several extensions of the pQCD collinear framework have been proposed. These models take into account the possible spin-dependent transverse components of parton momentum (Sivers effect [4]), the possible spin-dependent fragmentation of a scattered polarized parton (Collins effect [5]), or higher twist effects where transverse phenomena related to the previous approaches are included in the hard scattering term of a collinear calculation [6, 7]. Each of these approaches is a natural extension of the original factorized pQCD framework. A wide range of high energy polarized scattering experiments have been motivated by the need to determine which of these or other extensions of collinear pQCD is most consistent with data [8–12].

For more than 20 years, we have known that the transverse asymmetries in forward pion production depend critically on the isospin projection ( $I_3$ ) of the produced mesons relative to that of the parent hadron. In proton scattering, the asymmetry for  $\pi^-$  mesons, which largely originate from fragmentation of minority down quarks, has the opposite sign relative to the asymmetries for  $\pi^+$  and  $\pi^0$  mesons, produced from the predominate up quarks. In this letter, we report for the first time at  $\sqrt{s} = 200$  GeV the transverse single-spin asymmetry for the  $\eta$  meson, another member of the pseudo-scalar octet that has the same isospin projection as the  $\pi^0$  ( $I_3 = 0$ ). In addition, we report the differential cross section for

$\eta$  production in the region where the spin asymmetry is measured.

We emphasize that understanding an asymmetry result requires knowledge of the production cross section for the corresponding process. Traditional collinear pQCD has been successful in explaining the latter for various processes, which can be considered an applicability test of the pQCD framework. The former, on the other hand, requires the aforementioned extensions of the traditional approach. Consequently, the measurement of both quantities for a particular process provides the connection between the more conventional collinear pQCD and the various extensions of it.

For  $\pi^0$  production, recent STAR measurements of the forward cross section are consistent with next-to-leading-order (NLO) pQCD calculations in the region where the transverse spin asymmetry is large [8, 13, 14]. However, these results do not cover the large Feynman- $x$  region where the acceptance for the  $\eta$  decaying into two photons becomes large. In this letter, we have extended the analysis of the  $\pi^0$  cross section and  $A_N$  to much larger  $x_F$ , up to  $x_F$  of 0.75. This allows us to directly compare the spin asymmetries and cross sections for the  $\pi^0$  and  $\eta$  mesons in the same kinematic region.

The STAR Forward Pion Detector (FPD) is a modular lead glass calorimeter located in the very forward region of the interaction region at the Relativistic Heavy Ion Collider (RHIC) at Brookhaven National Laboratory. Two main modules are placed on either side of the beam line, with the average pseudo-rapidity of 3.7. Each module contains 49 glass columns, forming a  $7 \times 7$  square array. Each column is approximately 18 radiation lengths deep, and slightly more than 1 Moliere radius wide. The data were collected during RHIC year 2006 transversely polarized proton running, with an integrated luminosity of  $6.8 \text{ pb}^{-1}$  [8]. The average polarization was  $(56 \pm 2.6)\%$  for the beam facing the east FPD, with which the data for this analysis were taken. Events were recorded only

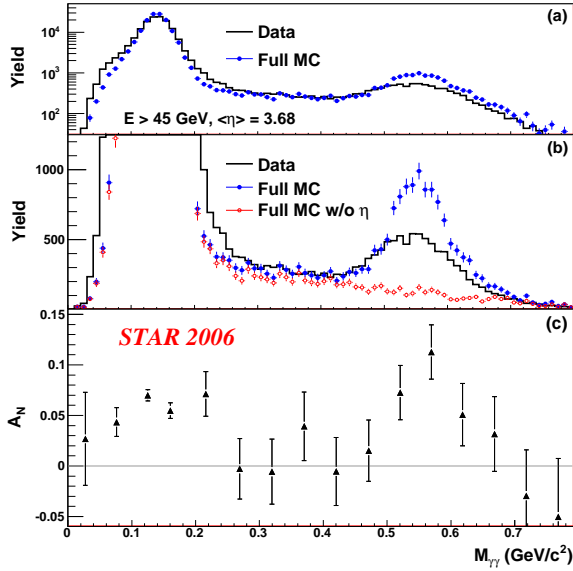


FIG. 1: (a) Di-photon invariant mass,  $M_{\gamma\gamma}$ , distributions in data and simulation for  $E > 45 \text{ GeV}$ , with the “center cut” as defined in Eq. (2). Simulation was normalized to have the same number of events as the data in the  $\pi^0$  mass region ( $0.08 < M_{\gamma\gamma} < 0.19 \text{ GeV}/c^2$ ). (b) Same as (a), but plotted using an expanded linear scale to illustrate the  $\eta$  mass region. For the red hollow points, the  $\eta$  signal was removed from the simulation at the PYTHIA level. (c) Transverse single-spin asymmetry,  $A_N$ , vs.  $M_{\gamma\gamma}$  for the above mass distribution. The error bars are statistical uncertainties only.

when the total ADC count in either of the two modules was greater than a fixed threshold, which was nominally equivalent to 30 GeV. Photons reconstructed less than one quarter of a cell width away from the detector edge were discarded. Only those events with two reconstructed photons were analyzed. The loss of yield due to this requirement has been corrected for the cross-section measurement. The STAR Beam Beam Counter (BBC) on the away side (west) was used to reject the single-beam background. The near side (east) BBC was not required to produce a signal, as most of the analyzed events already have more than half the beam energy deposited in the east FPD.

The previous STAR publication of  $\pi^0$   $A_N$  [8] utilized this data set. However, due to a larger separation of the decay photons, the acceptance for the  $\eta$  meson lies mostly above an  $x_F$  of 0.5, which is near the previous upper limit of the  $x_F$  coverage for the  $\pi^0$ . The Moliere radius and transverse cell size are similar to the typical separation of two decay photons from a 60 GeV  $\pi^0$  at the front surface of the FPD. The discrimination between single photon and  $\pi^0$  clusters above 60 GeV has required improvement in analysis methods used in previous STAR publications. The current analysis improves upon the previous one in a number of aspects, by extending the  $x_F$  reach for the  $\pi^0$  while ensuring a higher precision calibration required

by cross-section measurements.

More significantly, the GEANT simulation of the electromagnetic shower in the FPD is now based on the tracking of optical photons produced by the Čerenkov effect. Compared to the previous method based on charged particle energy loss, this simulation produces a much better agreement with the data in almost all aspects, including shower shape, energy resolution, and the observed shift in gain as a function of photon energy. In addition, the separation of single photon clusters from clusters that contain two merged photons was greatly improved by a revised cluster moment analysis. Previously, the photon content of a cluster was determined by analyzing its second moment of energy in relation to its total energy. In the revised scheme, the second moment is calculated in logarithm of energy, with a minimum energy requirement for each tower to suppress small fluctuations. The new method provides significantly improved sensitivity to the topological differences between single and double photon clusters. A more advanced parameterization of the shower shape, including the effects of incident angle, also contributes to the overall improvement of the event reconstruction. As a result, the maximum energy below which single photons and  $\pi^0$ 's can be reliably separated has been increased from 55 GeV to 80 GeV.

The top two panels of Fig. 1 show data-simulation comparisons of the di-photon invariant mass spectra. The “center cut”, so named because it covers roughly the central region of the FPD acceptance, is imposed on all event samples in order to enhance the  $\eta$  acceptance relative to the background. It is defined as

$$(y - 3.65)^2 + \tan^2(\phi) < 0.15, \quad (2)$$

where  $y$  is the pseudorapidity relative to the polarized beam and  $\phi$  is the azimuthal angle of the di-photon center of mass. A full simulation based on PYTHIA version 6.222 and GEANT 3 was compared to the data. The reflectivity and absorption properties of the aluminized mylar wrapped glass cells were varied to minimize the discrepancies between the photon shower shape in the simulation and that measured in the data. While detailed knowledge of the glass-mylar interface remains a limiting factor in the precise modeling of the shower development, the agreement in the widths of mass peaks between the simulation and data has been improved significantly over previous analyses. Furthermore, the data-simulation agreement in the continuum region between the  $\pi^0$  and  $\eta$  peaks is very good, allowing for a simulation based background estimation for the  $\eta$  signal. Correction factors have been applied to account for the remaining data-simulation discrepancies in mass resolution. The  $\eta$  to  $\pi^0$  ratio is higher in the simulation than in the data, reflecting limitations of PYTHIA in the forward region. Also shown is the invariant mass dependence of  $A_N$ , which exhibits a clear suppression in the continuum region.

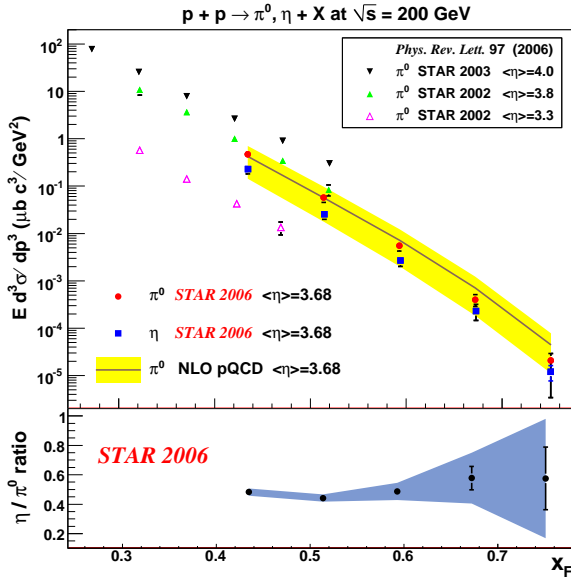


FIG. 2: Differential production cross sections for  $\pi^0$  and  $\eta$  at average pseudorapidity of 3.68 with the center cut. Also shown are the previously published STAR results for similar kinematics [14] and a NLO pQCD calculation of the  $\pi^0$  cross section. The yellow band represents the uncertainty in the calculated cross section due to scale variations. The  $\eta$  to  $\pi^0$  cross-section ratio is shown in the bottom panel. The blue band represents the combined statistical and systematic uncertainties.

the simulation, this mass region is dominated by approximately equal contributions from a pair of photons from two different  $\pi^0$  decays and a charged hadron combined with a photon.

The energy resolution of the FPD is estimated to be about 7 to 8 % of the total energy based on the comparison of invariant mass and di-photon separation distributions between data and Čerenkov shower simulation. Coupled to the rapidly falling cross section as a function of energy, the limited resolution causes substantial bin migration when measuring cross sections. We unfold the effect of the energy smearing by constructing a smearing matrix based on simulation that maps the true energy of an event to the apparent energy, and applying it to an ensemble of all possible energy distributions satisfying a smoothness requirement. The true energy distribution is identified as the one that transforms to an apparent energy distribution that most closely resembles the measured distribution, based on  $\chi^2$  analysis.

The upper panel of Fig. 2 shows the differential cross-sections for  $\pi^0$  and  $\eta$ . The center cut (Eq. 2) was imposed on both mesons. Also shown are the previously published STAR results for the  $\pi^0$  cross section in similar kinematic regions. The yellow band corresponds to the NLO pQCD theory prediction for the  $\pi^0$  cross section, [15] based on the CTEQ6M5 parton distribution function [16] and DSS fragmentation function [17]. The uncertainty for the the-

ory prediction was obtained by increasing the factorization and renormalization scales from  $\mu = p_T$  to  $\mu = 2p_T$ . We note that the DSS fragmentation function includes in the fit the previously published STAR results at pseudorapidity of 3.3 and 3.8 [13], along with other RHIC results. The error bars include both statistical and systematic uncertainties. The statistical uncertainties are indicated by the colored error bars, which are visible only in the very last bins. The major sources of systematic uncertainties are the absolute calibration uncertainty of 3%, which dominates the  $\pi^0$ , and the uncertainty from the unfolding process, which dominates the  $\eta$  at high energies. The normalization uncertainty was conservatively estimated at 20%.

The lower panel of Fig. 2 shows the  $\eta$  to  $\pi^0$  cross-section ratio. The error bars indicate the statistical uncertainty, while the blue error band includes both statistical and systematic uncertainties. The uncertainty in the absolute calibration is common to  $\pi^0$  and  $\eta$ , and has minimal effect on the cross-section ratio. However, because the two mesons often populate different parts of the detector, the relative energy calibration uncertainty of 1.5% is a significant part of the systematic uncertainty.

In pQCD, large- $x_F$  production of both  $\pi^0$  and  $\eta$  arises from hard-scattered partons fragmenting into mesons with large momentum fraction  $z$  (ratio of hadron momentum to the momentum of its parent parton). The fragmentation process is often thought to be universal, as evidenced by the fact that a single set of pion fragmentation functions explains a wide variety of RHIC data [18–20]. There is less known about large  $z$  fragmentation into  $\eta$  mesons, but in a recent global analysis of previous measurements of jet-like events, the ratio of  $\eta$  to  $\pi^0$  production was found to be close to 50% [21], consistent with our findings. While there are currently no NLO pQCD predictions for forward  $\eta$  production, it is likely that the pQCD calculations of  $\pi^0$  and  $\eta$  cross sections will be similar except for the differences in fragmentation.

Figure 3 shows the analyzing power as a function of  $x_F$  for  $\pi^0$  and  $\eta$ , after correcting for the underlying background. Also shown is the previous STAR result for  $\pi^0 A_N$  at lower  $x_F$ , which utilized the same data set as the current analysis but without the center cut. The two  $\pi^0$  results are consistent within their correlated errors. The background correction, which only significantly affects the  $\eta$  asymmetry at medium energy, is obtained from the assumed analyzing power of  $0.005 \pm 0.016$  for the background, extracted from Fig. 1(c). The error bars indicate statistical errors only, while the error bands indicate the systematic errors. The main source of the systematic uncertainty is the background correction, and polarization uncertainty is negligible in comparison.

In conclusion, STAR has measured the  $x_F$  dependences of the cross section and transverse single-spin asymmetries for  $\pi^0$  and  $\eta$  mesons produced at an average pseudorapidity of 3.68 in  $\sqrt{s} = 200$  GeV polarized proton

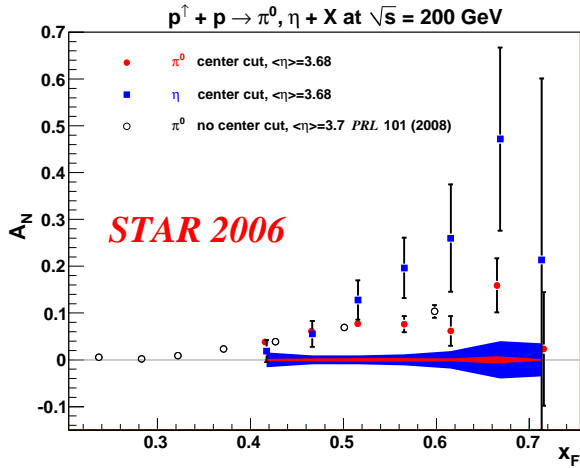


FIG. 3:  $A_N$  vs.  $x_F$  at average pseudorapidity of 3.68 for  $\pi^0$  and  $\eta$ . Also shown are the previously published results for  $\pi^0$  at lower  $x_F$ , derived from the same data set but without the center cut [8]. The error bars are statistical uncertainties only. The red (blue) error band indicates the systematic uncertainty for  $\pi^0$  ( $\eta$ ).

collisions. Over the region  $0.5 < x_F < 0.75$ ,  $A_N$  for the  $\eta$  meson is 2.5 standard deviations larger than that of the  $\pi^0$ . The measured  $\pi^0$  cross section is consistent with a pQCD prediction for the same kinematic region in which the spin asymmetry was measured. Although there are no theoretical predictions for the  $\eta$  cross section for these kinematics, we note that the  $\eta/\pi^0$  cross-section ratio is similar to previous measurements for mid-rapidity production at the same  $\sqrt{s}$  [18, 21, 22]. The agreement strongly suggests that the surprisingly large  $\eta$  asymmetry can be understood within the framework of pQCD. The large difference in  $A_N$  for  $\pi^0$  and  $\eta$  mesons is of particular interest given their similar up and down quark content, with wave-functions of both mesons containing  $u\bar{u}$  and  $d\bar{d}$  pairs. The  $\eta$  differs from the  $\pi^0$  mainly in that it is in an isospin singlet state, and that it is expected to contain strangeness. In addition, the latter results in the  $\eta$  being significantly more massive than the  $\pi^0$ . Currently, there is only one theoretical model that can generate an  $\eta$  asymmetry that is substantially larger than that of the  $\pi^0$  [23]. The model includes a sizable initial-state twist-3 effect for strange quarks, which results in an  $\eta$  asymmetry that rises to about 12 % at  $x_F$  of 0.4, but agrees quantitatively with the data for  $x_F > 0.5$ . It is yet unknown if this difference in  $A_N$  can arise from the fragmentation process via the Collins effect. Understanding the precise nature of these asymmetries can be

aided greatly by complementary measurements of  $A_N$  for non-hadronic final states, such as jets and prompt photons. The STAR Forward Meson Spectrometer (FMS), a significantly larger lead-glass calorimeter that replaced the west FPD in the year 2008, can provide the necessary acceptance for these measurements, along with a much broader kinematic coverage.

- 
- [1] G. L. Kane, J. Pumplin, and W. Repko, Phys. Rev. Lett. **41**, 1689 (1978).
  - [2] D. L. Adams et al. (E581), Phys. Lett. **B261**, 201 (1991).
  - [3] D. L. Adams et al. (FNAL-E704), Phys. Lett. **B264**, 462 (1991).
  - [4] D. W. Sivers, Phys. Rev. **D41**, 83 (1990).
  - [5] J. C. Collins, Nucl. Phys. **B396**, 161 (1993), hep-ph/9208213.
  - [6] J.-w. Qiu and G. F. Sterman, Phys. Rev. Lett. **67**, 2264 (1991).
  - [7] Z.-B. Kang, J.-W. Qiu, W. Vogelsang, and F. Yuan, Phys. Rev. **D83**, 094001 (2011), 1103.1591.
  - [8] B. I. Abelev et al. (STAR), Phys. Rev. Lett. **101**, 222001 (2008), 0801.2990.
  - [9] S. S. Adler et al. (PHENIX), Phys. Rev. Lett. **95**, 202001 (2005), hep-ex/0507073.
  - [10] I. Arsene et al. (BRAHMS), Phys. Rev. Lett. **101**, 042001 (2008), 0801.1078.
  - [11] A. Airapetian et al. (HERMES), Phys. Rev. Lett. **94**, 012002 (2005), hep-ex/0408013.
  - [12] M. Alekseev et al. (COMPASS), Phys. Lett. **B673**, 127 (2009), 0802.2160.
  - [13] J. Adams et al. (STAR), Phys. Rev. Lett. **92**, 171801 (2004), hep-ex/0310058.
  - [14] J. Adams et al. (STAR), Phys. Rev. Lett. **97**, 152302 (2006), nucl-ex/0602011.
  - [15] W. Vogelsang, Private Communication (2011).
  - [16] W. K. Tung et al., JHEP **02**, 053 (2007), hep-ph/0611254.
  - [17] D. de Florian, R. Sassot, and M. Stratmann, Phys. Rev. **D75**, 114010 (2007), hep-ph/0703242.
  - [18] B. I. Abelev et al. (STAR), Phys. Rev. **C81**, 064904 (2010).
  - [19] S. Adler et al. (PHENIX), Phys. Rev. Lett. **91**, 072303 (2003).
  - [20] A. Adare et al. (PHENIX), Phys. Rev. **D76**, 051106 (2007).
  - [21] C. A. Aidala, F. Ellinghaus, R. Sassot, J. P. Seele, and M. Stratmann, Phys. Rev. **D83**, 034002 (2011), 1009.6145.
  - [22] S. S. Adler et al. (PHENIX), Phys. Rev. **C75**, 024909 (2007), nucl-ex/0611006.
  - [23] K. Kanazawa and Y. Koike (2011), 1104.0117.